



## Two-component Marangoni-contracted droplets: friction and shape

Journal:	<i>Soft Matter</i>
Manuscript ID	SM-ART-12-2017-002361.R4
Article Type:	Paper
Date Submitted by the Author:	16-Aug-2018
Complete List of Authors:	Benusiglio, Adrien; Stanford University Graduate School of Education, Bioengineering; Otherlab Cira, Nate; Stanford University; Rowland Institute at Harvard Prakash, Manu; Stanford University, Bioengineering

## Two-component Marangoni-contracted droplets: friction and shape

Adrien Benusiglio,<sup>1,2,\*</sup> Nate J. Cira,<sup>1,3,†</sup> and Manu Prakash<sup>1</sup>

<sup>1</sup>*Department of Bioengineering, Stanford University,  
450 Serra Mall, Stanford, California 94305, USA*

<sup>2</sup>*Otherlab, 3101 20th Street, San Francisco, California 94110, USA*

<sup>3</sup>*Rowland Institute, Harvard University, 100 Edwin Land Blvd, Cambridge, MA 02142, USA*

(Dated: August 16, 2018)

When a mixture of propylene glycol and water is deposited on a clean glass slide, it forms a droplet of a given apparent contact angle rather than spreading as one would expect on such a high-energy surface. The droplet is stabilized by a Marangoni flow due to the non-uniformity of the components' concentrations between the border and the apex of the droplet, itself a result of evaporation. These self-contracting droplets have unusual properties such as absence of pinning and the ability to move under an external humidity gradient. The droplets' apparent contact angles are a function of their concentration and the external humidity. Here we study the motion of such droplets sliding down slopes and compare the results to normal non-volatile droplets. We precisely control the external humidity and explore the influence of the volume, viscosity, surface tension, and contact angle. We find that the droplets suffer a negligible pinning force so that for small velocities the capillary number ( $Ca$ ) is directly proportional to the Bond number ( $Bo$ ):  $Ca = Bo \sin \alpha$  with  $\alpha$  the angle of the slope. Lastly we study the successive shapes the droplets take when sliding at larger and larger velocities.

### INTRODUCTION

When a small droplet of a pure, non-volatile liquid is deposited on a surface, it spreads until the three phase contact line around the droplet reaches an equilibrium contact angle  $\theta$  with the surface. In the case that the liquid totally wets the surface (a high-energy surface for the liquid), there is no equilibrium, and the droplet continuously spreads, with a dynamically decreasing contact angle resulting from a balance of surface tension and viscous dissipation [1, 2]. If the liquid is partially wetting, the contact angle is dictated by Young's law [3]. Young's law is a horizontal balance between three forces or minimization of three surface energies associated with three interfaces: the liquid/air, liquid/substrate and substrate/air interfaces [4]. It was theoretically and experimentally shown that a non-uniform surface/air or liquid/air energy could put the droplets in motion [5–7]. Recently Cira *et al.* [8, 9] showed that a two-component droplet of the right miscible liquids will not spread on a high-energy surface, but instead will form a well defined droplet with an apparent contact angle  $\theta$ . The stabilization of the droplet is due to evaporation of one component that creates a gradient of concentration in the droplet, itself at the origin of a Marangoni flow working against the spreading force, so that the droplet is 'Marangoni-contracted' [10–13]. Such droplets move in response to external humidity gradients that modify their evaporation [14], and thus can attract each other [8].

The motion of a typical sessile droplet of viscosity  $\eta$ , surface tension  $\gamma$ , volume  $V$  and density  $\rho$  is limited by its contact angle hysteresis  $\Delta\theta$  due to microscopic geometrical or chemical inhomogeneities that induce pinning [15–17]. For example a small droplet presenting a small

mean contact angle  $\theta$  and contact angle hysteresis placed on an incline will only move under a gravitational force  $\rho V g \sin \alpha$  larger than the pinning force  $V^{1/3} \gamma \theta \Delta\theta$ , with  $\alpha$  the angle of the slope with the horizontal and  $g$  the gravitational acceleration [16, 18, 19]. Above the force threshold the droplets then move at a velocity  $U$  such that the capillary number ( $Ca = \frac{\eta U}{\gamma}$ ) that compares viscous forces and surface tension is a linear function of the Bond number ( $Bo = \frac{V^{2/3} \rho g}{\gamma}$ ) that compares gravity and surface tension, times  $\sin(\alpha)$  [20, 21]. For usual sessile droplets, contact angle hysteresis is strongly reduced on super-hydrophobic surfaces, and can even be cancelled for liquid-infused also known as "SLIP" surfaces [22–24]. The droplet friction nature in the later case is a function of the ratio between the droplet and the oil viscosity [25]. Here surprisingly the self-contracted droplets do not suffer from pinning, as they move on a film of their own constituents that spreads around them. The pinning cancelation of Marangoni contracted droplets on high-energy substrates has hardly been reported in the literature. It was described by Huethorst and Marra [26], for droplets of water in a 1-methoxy-2-propanol vapor atmosphere that maintain a constant static contact angle. In the system we present here, there is no need to place the droplets in a specific atmosphere as they self induce a Marangoni contraction through evaporation. We can control the contact angle and viscosity of the droplets by tuning their concentration and the external humidity on a large range.

In this letter we study in detail the friction the evaporative Marangoni-contracted droplets feel running down a slope, as a function of the parameters ( $V, \theta, \gamma, \eta$ ), first for small slopes where droplets do not deform, then for larger slopes on which the droplet shape changes, comparing the

droplets to regular non-volatile sessile droplets. First we briefly discuss how we can set  $\theta$ .

## RESULTS AND DISCUSSION

The droplets are composed of propylene glycol *PG* and distilled water, with a concentration  $C$  noted as % of the *PG* volume over the total volume. The mixture properties are extracted from the literature [27]. We first measured  $\theta$  as a function of the relative humidity  $RH$  and  $C$ . The experiments were done in a humidity controlled chamber built in the laboratory with two sealed glove access ports. The relative humidity can be set from 10% to 95%. The droplets are deposited with a calibrated pipet on clean fully hydrophilic glass slides, see [8] for details. The contact angle  $\theta$  was measured with a reflectometry setup [28] integrated with the box, see [8] for details. Droplets of both pure liquids spread, as expected on such a high-energy surface, but adding only a small amount of *PG* to water (0.01 %) is enough to obtain a stable  $\theta$  around 5°. The contact angle of 0.5  $\mu\text{L}$  droplets as a function of  $C$  for three different  $RH$  is shown on Fig. 1 (a).  $\theta$  increases to a maximum and decreases back to zero as the droplet concentration is increased. The amplitude of the curve and the maximum  $C$  for which a stable droplet is observed both decrease with  $RH$ . Varying  $RH$  for  $C = 10\%$ , we observe that  $\cos\theta$  increases linearly with the humidity, with  $\theta$  from 14 to 6 degrees [Fig. 1 (b)]. At a fixed humidity we observe that  $\theta$  decreases slightly with  $V$  from 0.5 to 4  $\mu\text{L}$  [Fig. 1 (c)]. In the following we will use values of  $\theta$  measured for droplets of 0.5  $\mu\text{L}$ . The radius of the droplet  $R$  will be estimated assuming a spherical cap shape and the contact angle of  $V = 0.5 \mu\text{L}$  droplets, as  $\theta$  variation with volume only gives a 3% error on the estimation of  $R$  for the larger 4  $\mu\text{L}$  droplets.

A sessile droplet deposited on a surface evaporates faster from the borders than from the center because of thermal [29, 30] and mainly geometrical [31, 32] effects. For these two-component mixtures the droplet starts by spreading on the time scale of one second after deposition before building up back to a radius constant on the time scale of one minute. We observe under the microscope that a thin film surrounds the droplet and spreads hundreds of microns from the droplet [8]. Interferometry measurements suggest that the film thickness increases from less than 100 nm to 300 nm as the droplet concentration is increased, orders of magnitude thicker than typical precursor films (Fig. 2). As for a sessile droplet, the border of the droplet and the thin film evaporate faster than the center [33]. We will assume that only water is evaporating as it is 100 times more volatile than *PG* [34]. Due to faster evaporation and thickness,  $C$  increases in the thin film and border, and remains constant in the bulk on the minute time-scale (in the following, all

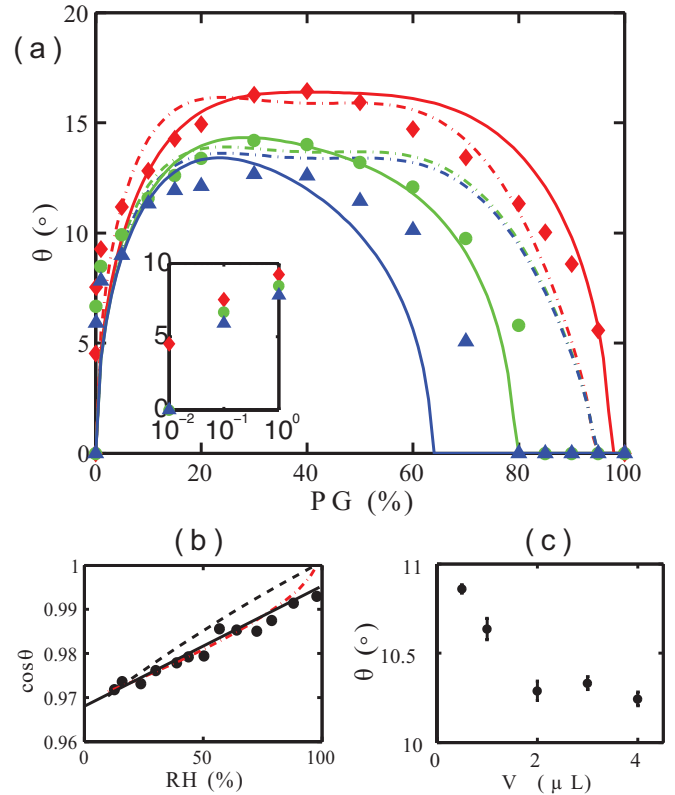


FIG. 1. (a)  $\theta$  of 0.5  $\mu\text{L}$  two-components droplets as a function of  $C$  for three  $RH$  (triangles:  $RH = 70\%$ , circles:  $RH = 51\%$ , diamonds:  $RH = 10\%$ ). The solid lines represent the best fit of the model at each  $RH$  for  $C = 10\%$ , with from the lowest to the largest  $RH$  (blue, green and red):  $K = 0.17, 0.31, 0.50$ . The dashed lines represent the best fit with the model from [8], same color code. Inlet: zoom on low concentrations. (b) Measured  $\cos\theta$  as a function of  $RH$  for  $C = 10\%$ , 0.5  $\mu\text{L}$  droplets. The best linear fit is shown with a solid line, our model with a dashed line and the model from Karpitschka et al. [13] with a red dashed and dot line. (c)  $\theta$  as a function of  $V$  for  $C = 10\%$  droplets at  $RH = 43\%$ . The error bars in c) represent the standard error with minimum 3 measurements.

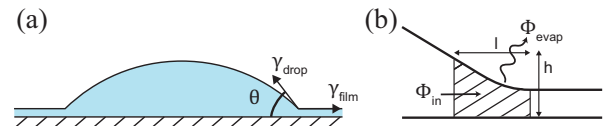


FIG. 2. (a) Representation of the droplet and its surrounding thin film and notations. (b) Definition of the notations describing the meniscus between the bulk droplet and the thin film.

measurements are done in the first minute). Because  $\gamma$  is monotonically decreasing with  $C$ , the gradient of concentration creates a gradient of surface tension that drives a Marangoni flow along the droplet surface from the border to the apex.

Following from [8], we construct a flux based model to capture the contact angle. Departing from [8], we incorporate Raoult's law into the evaporative flux term. We assume that  $C$  quickly varies between the droplet and the film in a transition region or meniscus of typical length  $l$  and thickness  $h$  (Fig. 2), and is quasi-constant elsewhere. The force equilibrium in the horizontal direction gives:

$$\gamma_{\text{bulk}} \cos \theta = \gamma_{\text{film}} \quad (1)$$

with  $\gamma_{\text{bulk}}$  and  $\gamma_{\text{film}}$  the surface tension of the droplet and the thin film respectively. We write the conservation of water in the transition region. At equilibrium, the local relative humidity above the thin film is equal to the molar concentration of water  $z_w$ , and we assume that the evaporative flux is proportional to the difference between the local relative humidity and  $RH$  (introducing Raoult's law and improving the estimation done in [8]): there is no evaporation if  $z_w \leq RH$ , and otherwise the evaporation happens at the rate per unit area  $\Phi_{\text{evap}} = (z_w - RH)A_w$ , with  $A_w$  the evaporative flux per unit area of pure water at  $RH = 0\%$ . We estimate the water volume fraction in the transition region  $x_{\text{wfilm}}$  assuming that a flux per unit area  $\Phi_{\text{in}}$  of liquid of initial water volume fraction  $x_w$  is flowing from the droplet to the thin film. The volume of the transition region without evaporation is  $V_t = \Phi_{\text{in}} h dr dt$  with  $dr$  an infinitesimal arc along the droplet perimeter and  $dt$  the time to fill  $V_t$ . The volume of water evaporating during this time is  $V_{\text{evap}} = \Phi_{\text{evap}} l dr dt$ . After time  $dt$ ,  $x_w V_t - \Phi_{\text{evap}} l dr dt$  water is left in the transition region, which has total volume  $\Phi_{\text{in}} h dr dt - \Phi_{\text{evap}} l dr dt$ , giving the water fraction of the transition region  $x_{\text{wfilm}} = \frac{x_w V_t - \Phi_{\text{evap}} l dr dt}{\Phi_{\text{in}} h dr dt - \Phi_{\text{evap}} l dr dt}$ . It can be rewritten:

$$x_{\text{wfilm}} = \frac{x_w - (z_w - RH) K}{1 - (z_w - RH) K} \quad (2)$$

with the non-dimensional parameter  $K = \frac{A_w l}{\Phi_{\text{in}} h}$ . Equation (2) predicts a surface tension difference of maximum 3% between the bulk and the thin film and a viscosity difference of maximum 14%. Combining Equations (1) and (2), for a given  $RH$ , we choose the best  $K$  to fit the measurement, and we observe that the model captures the  $\theta$  trend and predicts the maximum  $C$  up to which we observe a stable droplet (Fig. 1 a), with a better precision than what was proposed previously [8]. Keeping a constant  $K$  also partially predicts the amplitude variation as a function of  $RH$ . For example, for droplets of 10%  $PG$ , the model predicts a quasi-linear evolution of  $\cos \theta$  with  $RH$  in the range  $RH = 10 - 80\%$ , for  $K = 0.21$ , but with a larger slope than the best linear fit of the data (Fig 1 b). The model by Karpitschka et al. [13] resolves time dependent mass transport equations in lubrication approximation taking into account capillary, Marangoni, and diffusive fluxes from an evaporating droplet, and fixing the thickness of the surrounding film

as the one of a precursor film. It proposes a relationship  $\theta \propto (RH_{\text{eq}} - RH)^{1/3}$  with  $RH_{\text{eq}}$  the relative humidity above which the droplet spreads completely, in good agreement with our measurements.

Having either measured the parameters of the Marangoni-contracted droplets as a function of  $RH$  and  $C$  ( $\theta$ ), or having access to them in the literature ( $\gamma$ ,  $\eta$ ), now we explore the role of these parameters on the friction a droplet feels moving down a slope. We first restrict ourselves to the range of  $V$  and  $\alpha$  for which the droplets do not noticeably deform. The choice of a  $PG$ /water droplet is at first glance unpractical since when  $C$  changes,  $\theta$ ,  $\gamma$  and  $\eta$  change. But it in fact reveals a powerful tool to estimate the role of each parameter, as  $\gamma$  is a monotonically decreasing function of  $C$ , when  $\eta$  is monotonically increasing. The droplets are deposited on a clean glass slide placed on a slope of angle  $\alpha$  from 0 to 45° enclosed in the humidity-controlled chamber.  $V$  ranges from 0.25 to 10  $\mu\text{L}$ . The motion is recorded from the top with a digital SLR camera. We observed that after accelerating on the millimeter scale, the droplets moved at constant  $U$  in the direction of the largest slope. For a given  $V$  and  $C$  we gradually increased  $\alpha$  and observed that  $U$  is a direct linear function of  $\sin \alpha$  (Fig. 3 a). We then varied the volume of the droplets and observed that larger droplets moved faster.

Two-component droplets of typical radius  $R = 1$  mm move at typical velocities  $U = 1$  mm/s, so that the Reynolds number is equal to  $\text{Re} = \frac{\rho R U}{\eta} \approx 1$  (when estimating  $\text{Re}$  on the thickness of the droplet  $\delta \approx \theta R$ ,  $\text{Re} \approx 0.2$ ). When the droplets slide down the slope, they are subject to a drag force due to the gradient of velocity from the surface of the droplet to the substrate. For a sessile droplet of small contact angle and small radius compared to the capillary length  $\kappa^{-1} = \sqrt{\gamma/\rho g}$ , the dissipation mainly happens in the wedge close to the moving contact line. The force per unit length is written, with  $U_n$  the velocity of the contact line normal to the droplet in the plane of motion:  $f_{\text{drag}} = \eta U_n \ln(b/a)/\theta$  [4], with  $\ln(b/a)$  the logarithmic ratio of a macroscopic length scale  $b$  (typically  $R$ ) and a microscopic length scale  $a$  at which the continuous matter description fails, such as the size of the molecules. A crude integration of the viscous force acting on a circular droplet is then  $F_{\text{drag}} = \pi R \eta U \ln(b/a)/\theta$ . The droplet is moving due to the gravitational force projected in the direction of motion  $F_{\text{prop}} = mg \sin \alpha$ . Equilibrating  $F_{\text{drag}}$  and  $F_{\text{prop}}$ , the velocity of the droplet is  $U = \frac{mg \sin \alpha A}{\pi \eta R}$ , with  $A = \theta/\ln(b/a)$ . A sessile droplet presenting a contact angle hysteresis would feel an additive pinning force, and the droplet would only move above that threshold force. Here we observe that the velocity is a linear function of  $\sin(\alpha)$  for droplets with  $C = 10\%$  and  $V = 0.25$  to 1.5  $\mu\text{L}$  [Fig. 3]. The linear fit of the velocity goes to

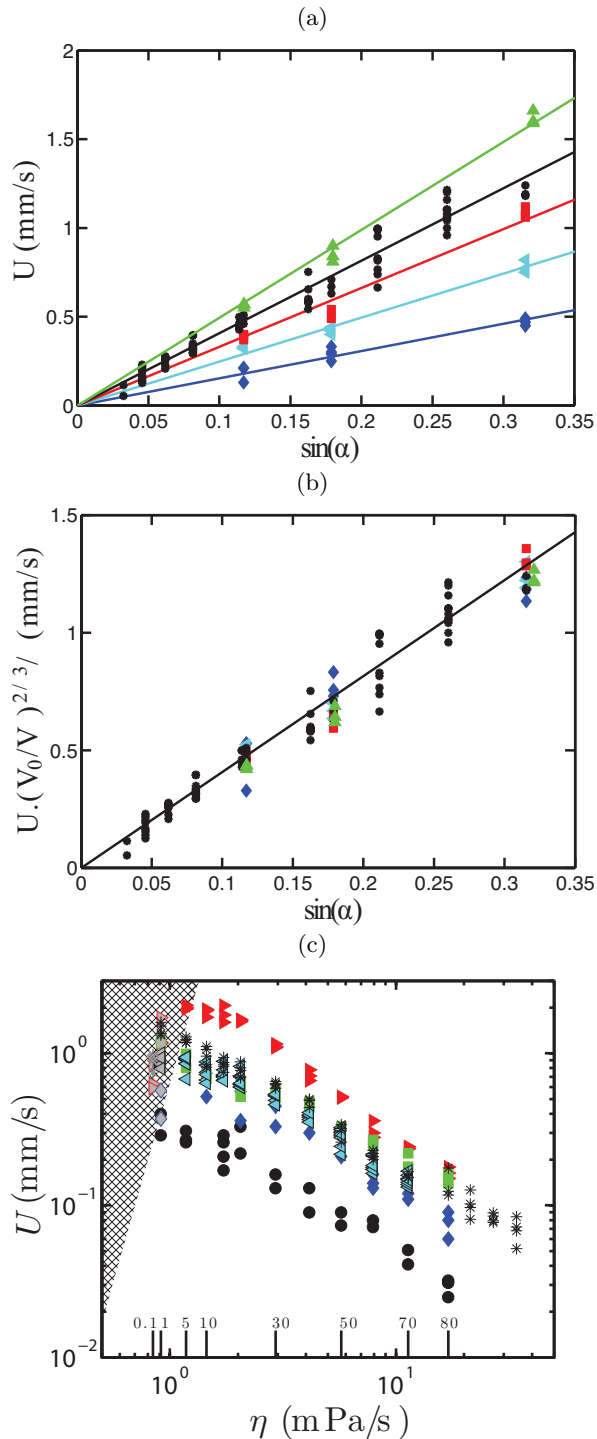


FIG. 3. (a)  $U$  as a function of  $\sin \alpha$  for  $C = 10\%$ . The dashed lines are best linear fits, the slope increasing with the  $V = 0.25, 0.5, 0.75, 1, 1.5 \mu\text{L}$ . (b) Rescaled velocity as a function of the slope.  $RH = 55\%$ . (c) Velocity as a function of the viscosity for various  $\alpha$ . The symbols represent the series done at a constant  $\alpha$  and  $RH$ , varying  $C$ . At ambient humidity ( $RH = 50 - 55\%$ ):  $\circ$ :  $\alpha = 3.73^\circ$ ;  $\diamond$ :  $7.7^\circ$ ;  $\triangleleft$ :  $11.3^\circ$ ;  $\square$ :  $13.5^\circ$ ;  $\triangleright$ :  $19^\circ$ . At reduced humidity:  $\star$ :  $RH = 10\%$ ,  $\alpha = 15.1^\circ$ . The region where pinning happens is grayed. The droplet concentration  $C$  is shown as a second horizontal axis above the main axis.

zero, showing that contrary to sessile droplets, the two-component droplets are not subject to pinning. The minimum rolling angle is unmeasurable, as it is the case with droplets on liquid-infused materials [25]. Assuming that the droplets are spherical caps,  $R \propto V^{1/3}$  and eventually  $U \propto V^{2/3} \frac{\rho g \sin \alpha A}{\eta}$ . We verify this scaling on Fig. 3 (b) where we plot the velocity rescaled by  $(V_0/V)^{2/3}$  with  $V_0 = 1 \mu\text{L}$ . This indicates that the viscous dissipation is a linear function of the radius and happens at the border of the droplet, as with typical sessile droplets with small contact angles. This is a different regime than for water droplets on liquid-infused surfaces for which the dissipation happens in the whole droplet and is thus a function of their area, rather than the radius, when the viscosity of the drop is large compared to that of the oil and the apparent contact angle close to  $90^\circ$  [25]. However this is similar to the other limit case for liquid-infused surfaces when the viscosity of the drop is small compared to that of the infused oil, where the dissipation happens in the oil meniscus around the drop, and is a function of the drop radius [25]. In the present case the meniscus is formed of the same liquid as the droplet (at a concentration only slightly different). From the velocity measurements, at  $RH = 55\%$ ,  $C = 10\%$  we extract the value of  $\ln(b/a) = 11.2$ , while an estimation based on the size of a molecule of water  $a = 152 \text{ pm}$  and  $R = 1 \text{ mm}$  gives  $\ln(b/a) = 15.7$  and on the size of a molecule of PG  $a \approx 495 \text{ pm}$  gives  $\ln(b/a) = 14.5$ . We then estimate a cut-off length  $a = 14 \text{ nm}$  over an order of magnitude larger than either components' molecular length, suggesting that for these droplets  $a$  may be set by something other than molecular length, such as the thickness of the film on which the droplets glide, or the length of the meniscus  $l$  between droplet and film [Fig. 2 (b)], again similarly to drops on liquid-infused surfaces.

We now extend the analysis to all stable (non wetting) concentrations to verify the influence of  $\theta$  and  $\eta$ . The range of stable concentration, contact angle and viscosity is: at  $RH = 55\%$   $C = 1\% - 80\%$ ,  $\theta = 8 - 13^\circ$  and  $\eta = 0.9 - 17.04 \text{ mPa}\cdot\text{s}$ ; at  $RH = 10\%$   $C = 0.1\% - 95\%$ ,  $\theta = 5.6 - 16^\circ$  and  $\eta = 0.84 - 34.17 \text{ mPa}\cdot\text{s}$ . On Fig. 3 (c) we plot the velocity as a function of concentration for different slopes. For a given  $\alpha$  and  $V$  we observed that  $U$  monotonically decreased with  $PG$  concentration, except for very low  $C$ . Careful examination revealed that at  $C \lesssim 1\%$  otherwise non-pinning droplets began pinning when moving on slopes with large  $\alpha$ , especially at higher humidities, leading to a reduction of velocity and scattering of measurements (indicated by hatched background and grayed points in Fig. 3 c). For these low concentrations, the limited  $PG$  content leads to a weaker Marangoni-contraction, evidenced by smaller contact angles. From our observations and simulations from Karpitschka *et al.* [13] the thin film is also thinner and extends to a smaller distance from the meniscus at low  $C$ .

One possible explanation leading to pinning is that the droplets in this region move faster than their surrounding films. The following analysis excludes the measurements done in this regime.

On Fig. 4 (a) we rescale the data to present the non-dimensional velocity  $\frac{\eta_0 R U}{mgA \sin \alpha} = \frac{U}{U_{\text{inf}} \eta_0 \sin \alpha} \propto \eta_0/\eta$ , with  $\eta_0$  the viscosity of pure water and  $U_{\text{inf}} \eta_0$  the theoretical velocity of non-deformed drops on a vertical surface, if they had the viscosity of pure water, as a function of  $\eta_0/\eta$ . Given that the larger than typical cutoff length  $a$  had suggested a potential role for the transition region in dissipation, we noted that if the dissipation was happening largely in the meniscus, the dissipative force might not be a function of  $\theta$ . To test this hypothesis, we also non-dimensionalized the velocity with a fixed value of  $A$ , that was not a function of  $\theta$ , and plotted the non-dimensional velocity as a function of the non-dimensional viscosity on Fig. 4 (b). We observe an almost linear fit of slope 1 for (b). The fit is worse for (a) as taking into account  $\theta$  bows the curve up for very low and very large  $C$ . The model using a fixed value of  $A$  gives a more linear fit to the data over a wider concentration range. We still observe a slight deviation from a power law fit, with droplets moving faster than predicted at high  $C$  (small  $\eta_0/\eta$ ). Again this reduced drag is consistent with observations [8] and simulations [13] of a more prominent film region at high  $C$ . It is our personal interpretation that globally (b) is a better fit, suggesting that the contact angle role on dissipation is minimal and that the dissipation happens in the transition region, whose geometry is minimally affected by  $\theta$ . This is again similar to droplets on a liquid-infused surface when the droplet is less viscous than the infused oil and the dissipation happens in the oil meniscus [25].

When a sessile droplet is running down a slope at larger and larger velocity, its receding contact line deforms from an oval shape to a corner shape, to a cusp emitting smaller droplets [20, 21]. The two-component droplet is stabilized by an internal flow that may reduce the deformation. We now study the motion and shape of the two-component droplets on large slopes on Fig. 5. For any  $C$ , as we increase  $\alpha$ , the back of the droplet deformed from an oval (a) to a cornered (b), to a cusped droplet emitting smaller droplets (c). The successive shapes were similar to what is observed for a sessile droplet [20, 21]. Qualitatively the equilibrium leading to deformation can be described as follows. Along the virtual contact line of the droplet, on the receding side the drag force per unit length is balanced by surface tension such as  $\eta \ln(b/a) U \cos \Phi = \gamma$ , with  $\Phi$  the angle between the normal to the droplet and  $U$  in the plane of motion (Fig. 5b). If  $\eta \ln(b/a) U < \gamma$  the receding contact line should stay non-deformed, and oth-

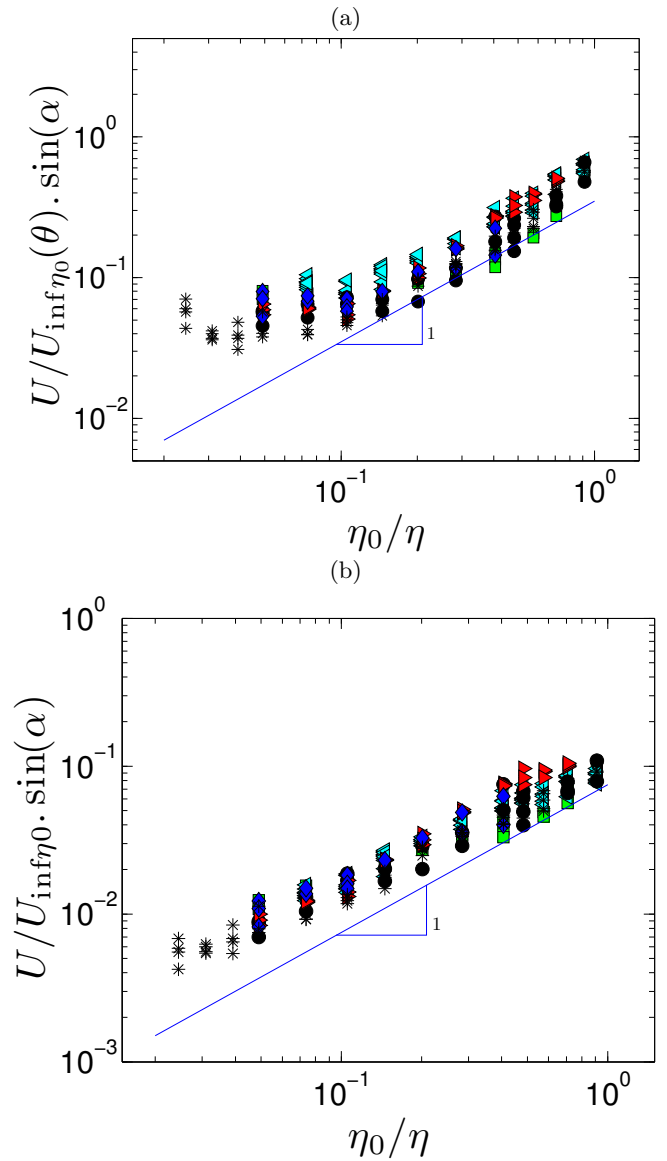


FIG. 4. Non-dimensional velocity as a function of the non-dimensional viscosity. (a)  $A$  is a function of  $\theta$ , (b)  $A$  is independent of  $\theta$ . Same symbols as in Fig. 3 (c).

erwise  $\cos \Phi = \frac{\eta U}{\gamma} = 1/Ca$ , which gives us the threshold for deformation  $Ca > 1$ . Plotting  $Ca$  versus  $Bo \sin \alpha$  on Fig. 5 (d) we observe that all the data collapses on a linear directing curve for small  $Bo \sin \alpha$ , as discussed in the introduction, and that goes to zero for small velocities because there is no contact angle hysteresis (here we define  $Bo$  as  $Bo = \frac{V \rho g}{R \gamma}$  because  $\theta$  and thus  $R$  are functions of the concentration). For larger  $Bo \sin \alpha$ , the droplet shape transitions and the slope of the directing curve increases. The slope increase can be interpreted as a drag reduction under the influence of the release of droplets [20]. The value of  $Ca$  for which the transition occurs is constant for a given  $C$  on a large range of  $V$  (Fig. 5 d), but is a function of  $C$ . More quantitatively

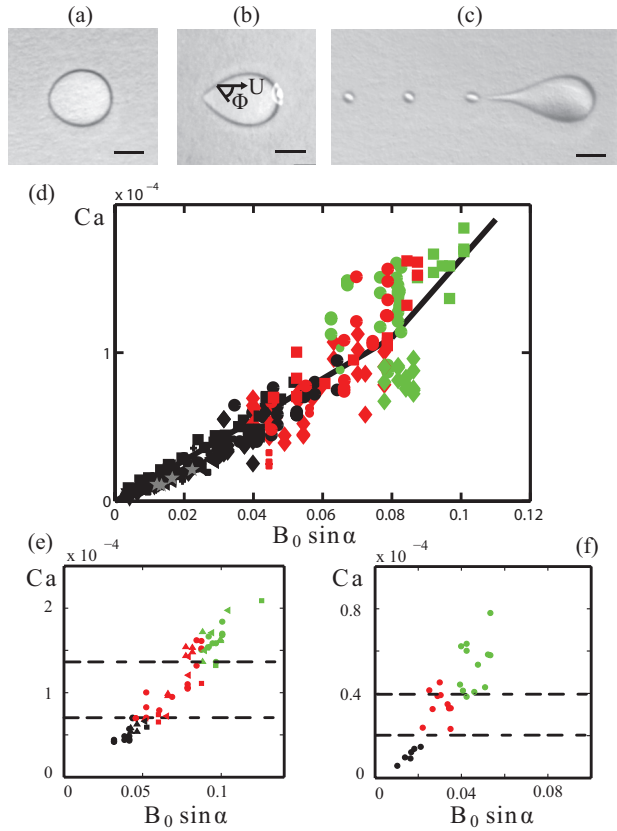


FIG. 5. Shapes of a  $1 \mu\text{L}$ ,  $C = 30\%$  droplet as the slope is increased: (a) oval, (b) conical, (c) pearling (the solid bar represents  $2 \text{ mm}$ ). (d)  $Ca$  as a function of  $B_0 \sin \alpha$ . Black, red and green symbols represent respectively droplets with an oval, conical and pearling receding contact line. The symbols represent different concentrations and volumes ( $RH = 50\%$ ): the volumes are only indicated for the  $C = 10\%$  droplet ( $\nabla$ :  $0.25 \mu\text{L}$ ,  $\Delta$ :  $0.5 \mu\text{L}$ ,  $\triangleright$ :  $0.75 \mu\text{L}$ ,  $\triangleleft$ :  $1 \mu\text{L}$ ,  $\diamond$ :  $1.5 \mu\text{L}$ , star hexagon:  $2 \mu\text{L}$ ).  $\square$ :  $C = 40\%$   $1.5 \mu\text{L}$ ; star pentagon:  $C = 5\%$ ,  $1.5 \mu\text{L}$ .  $+$ :  $C = 1\%$ ;  $\circ$ :  $C = 20\%$ , various volumes between  $0.5$  and  $2 \mu\text{L}$ . (e)  $C = 40\%$  droplets only ( $RH = 50\%$ ), the symbols represent different volumes:  $\circ$ :  $1.5 \mu\text{L}$ ,  $\Delta$ :  $3 \mu\text{L}$ ,  $\triangleleft$ :  $5 \mu\text{L}$ ,  $\square$ :  $10 \mu\text{L}$ . (f)  $C = 1\%$  droplet only,  $V = .5$  to  $3 \mu\text{L}$  ( $RH = 33\%$ ). In (e) and (f) the dashed lines highlight the thresholds of  $Ca$  for the successive shapes.

[20] predicts a deformation of the droplet above a critical capillary number  $Ca_c \sim \theta^3 / (9 \times \ln(b/a))$ . On figure 5 (e) we plot the same data for droplets of concentration  $C = 40\%$  only ( $\theta \approx 13^\circ$ ). Deformation of the droplet occurs for  $Ca$  above  $0.7 \times 10^{-4}$ , of the order of the estimated value of  $Ca_c = 1.2 \times 10^{-4}$ . Similarly on figure 5 (d), for  $C = 1\%$  at  $RH = 10\%$  ( $\theta \approx 8^\circ$ ) we observe a deformation for  $Ca$  above  $0.2 \times 10^{-4}$  very close to the expected value  $Ca_c = 0.2 \times 10^{-4}$ . We also observe that, as predicted, the second transition from cone to pearling droplet happens at twice  $Ca_c$  in both cases.

## CONCLUSION

Two-component mixtures of well chosen miscible liquids do not spread on high-energy surfaces but rather form stable droplets. Non-uniform concentration due to evaporation creates a Marangoni flow that stabilizes the droplets. A simple force balance model coupled with an estimation of the gradient of concentration gives a good picture of the Marangoni contraction process. Like typical sessile droplets, the two-component droplet velocity down a slope is a linear function of  $B_0 \sin \alpha$  for small  $Ca$ , but contrary to sessile droplets, they do not present contact angle hysteresis and pinning force, so that  $Ca = B_0 \sin \alpha$ . The droplets show an unmeasurable rolling angle, as it is the case with drops on liquid-infused surfaces. The influence of the static apparent contact angle of the droplets on the friction force remains to be fully understood but we suggest that it has a minimal role as the dissipation happens in the transition region between the droplet and its surrounding wetting film, which geometry is weakly affected by the contact angle, somehow similarly to what is observed for certain types of drops on liquid-infused surfaces. The absence of pinning is surprising, and the microscopic process making it possible remain to be determined but the presence of a thin film around the droplet seems to play a role. Droplets of very small viscosities moving on large slopes show some pinning as the film may not spread quickly enough to shield the droplet from the surface. Excluding the later case, when the Marangoni-contracted droplets run down slopes of increasing angle, their receding perimeter deforms from a circular arc to a cone at a given  $Ca$  and later deforms into a cusp that deposit smaller droplets, like regular sessile droplets. The first transition happens as predicted above a critical  $Ca$  of the order of  $Ca_c \sim \theta^3 / (9 \times \ln(b/a))$ , and the second transition at twice this value. The apparent contact angle then plays an important role on the shape transition, and a weaker one on the friction force.

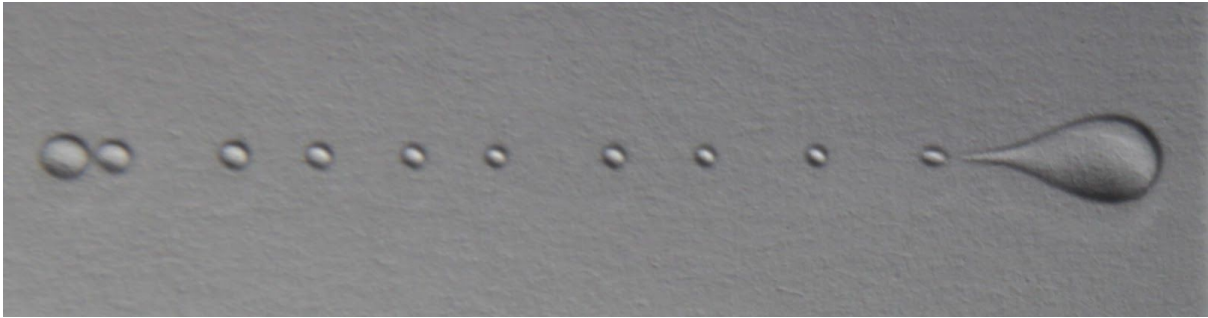
We wish to thank Stefan Karpitschka for helpful comments on the models and anonymous reviewers for feedback that strengthened the manuscript.

\* adrien.benusiglio@gmail.com

† cira@rowland.harvard.edu

- [1] L. Tanner, Journal of Physics D: Applied Physics **12**, 1473 (1979).
- [2] M. D. Lelah and A. Marmur, Journal of Colloid and Interface Science **82**, 518 (1981).
- [3] T. Young, Philosophical Transactions of the Royal Society of London, 65 (1805).
- [4] P.-G. De Gennes, Reviews of modern physics **57**, 827 (1985).
- [5] F. Brochard, langmuir **5**, 432 (1989).

- [6] T. Ondarçuhu and E. Raphaël, *Comptes rendus de l'Académie des sciences. Série 2, Mécanique, Physique, Chimie, Sciences de l'univers, Sciences de la Terre* **314**, 453 (1992).
- [7] M. K. Chaudhury and G. M. Whitesides, *Science* **256**, 1539 (1992).
- [8] N. Cira, A. Benusiglio, and M. Prakash, *Nature* (2015).
- [9] N. J. Cira, A. Benusiglio, and M. Prakash, *Physics of Fluids (1994-present)* **26**, 091113 (2014).
- [10] W. D. Bascom, R. L. Cottingham, and C. R. Singleterry (ACS Publications, 1964).
- [11] D. Pesach and A. Marmur, *Langmuir* **3**, 519 (1987).
- [12] Y. Tsoumpas, S. Dehaeck, A. Rednikov, and P. Colinet, *Langmuir* **31**, 13334 (2015).
- [13] S. Karpitschka, F. Liebig, and H. Riegler, *Langmuir* **33**, 4682 (2017).
- [14] T. K. Pradhan and P. K. Panigrahi, *Colloids and Surfaces A: Physicochemical and Engineering Aspects* **482**, 562 (2015).
- [15] C. Furmidge, *Journal of colloid science* **17**, 309 (1962).
- [16] E. Dussan V and R. T.-P. Chow, *Journal of Fluid mechanics* **137**, 1 (1983).
- [17] V. Dussan, *Journal of Fluid Mechanics* **151**, 1 (1985).
- [18] K. Kawasaki, *Journal of Colloid Science* **15**, 402 (1960).
- [19] D. Quéré, M.-J. Azzopardi, and L. Delattre, *Langmuir* **14**, 2213 (1998).
- [20] T. Podgorski, J.-M. Flesselles, and L. Limat, *Physical review letters* **87**, 036102 (2001).
- [21] N. Le Grand, A. Daerr, and L. Limat, *Journal of Fluid Mechanics* **541**, 293 (2005).
- [22] T.-S. Wong, S. H. Kang, S. K. Tang, E. J. Smythe, B. D. Hatton, A. Grinthal, and J. Aizenberg, *Nature* **477**, 443 (2011).
- [23] A. Lafuma and D. Quéré, *EPL (Europhysics Letters)* **96**, 56001 (2011).
- [24] J. D. Smith, R. Dhiman, S. Anand, E. Reza-Garduno, R. E. Cohen, G. H. McKinley, and K. K. Varanasi, *Soft Matter* **9**, 1772 (2013).
- [25] A. Keiser, L. Keiser, C. Clanet, and D. Quéré, *Soft Matter* **13**, 6981 (2017).
- [26] J. Huethorst and J. Marra, *Langmuir* **7**, 2756 (1991).
- [27] The viscosity of the mixture as a function of water volume fraction  $x_w$  is fitted by the polynomial:  $\eta = -163x_w^5 + 563x_w^4 - 775.93x_w^3 + 551.67x_w^2 - 217.87x_w + 43.504$ , from [? ]. The surface tension of the mixture as a function of  $x_w$  is fitted by the polynomial:  $\gamma = 25.955x_w^5 - 10.211x_w^4 - 5.087x_w^3 + 15.75x_w^2 + 12.452x_w + 35.47$ , from [? ].
- [28] C. Allain, D. Ausserre, and F. Rondelez, *Journal of colloid and interface science* **107**, 5 (1985).
- [29] W. Ristenpart, P. Kim, C. Domingues, J. Wan, and H. Stone, *Physical Review Letters* **99**, 234502 (2007).
- [30] X. Xu, J. Luo, and D. Guo, *Langmuir* **26**, 1918 (2009).
- [31] H. Hu and R. G. Larson, *The Journal of Physical Chemistry B* **106**, 1334 (2002).
- [32] J. Eggers and L. Pismen, *Physics of Fluids (1994-present)* **22**, 112101 (2010).
- [33] R. D. Deegan, O. Bakajin, T. F. Dupont, G. Huber, S. R. Nagel, and T. A. Witten, *Nature* **389**, 827 (1997).
- [34] G. O. Curme, *Glycols*, Vol. 114 (Reinhold, 1952).



We discuss in this paper the nature of the friction generated as a Marangoni-contracted drop glides on a slope.